Enriched finite elements for initial-value problem of transverse electromagnetic waves in time domain

M. Drolia[1], M.S. Mohamed[1], O. Laghrouche[1], M. Seaid[2], and J. Trevelyan[2]

[1]Institute for Infrastructure and Environment, Heriot-Watt University, Edinburgh EH14 4AS, UK
[2]School of Engineering and Computing Sciences, Durham University, Durham DH1 3LE, UK

Abstract

This paper proposes a partition of unity enrichment scheme for the solution of the electromagnetic wave equation in the time domain. A discretization scheme in time is implemented to render implicit solutions of systems of equations possible. The scheme allows for calculation of the field values at different time steps in an iterative fashion. The spatial grid is partitioned into a finite number of elements with intrinsic shape functions to form the bases of solution. Furthermore, each finite element degree of freedom is expanded into a sum of a slowly varying term and a combination of highly oscillatory functions. The combination consists of plane waves propagating in multiple directions, with a fixed frequency. This significantly reduces the number of degrees of freedom required to discretize the unknown field, without compromising on the accuracy or allowed tolerance in the errors, as compared to that of other enriched FEM approaches. Also, this considerably reduces the computational costs in terms of memory and processing time. Parametric studies, presented herein, confirm the robustness and efficiency of the proposed method and the advantages compared to another enrichment method.

Keywords. Electromagnetic Wave Equation; Finite Element; Partition of Unity; Time Domain Wave Problems; Enrichment Methods

1 Introduction

We live in an age in which we have harnessed electromagnetic waves to engineer a wide variety of products and systems on which modern societies have come to rely. Medical imaging devices, mobile communications and electrical power generation are just a few examples of technologies that are entirely reliant on electromagnetic phenomena. While the underlying differential equations that govern these phenomena were developed in the 19th century, their application to realistic engineering problems requires numerical approximations, and engineers continue to develop more advanced computational methodologies capable of delivering these approximations with higher fidelity and with efficient use of computational resources. In this paper we specifically address short wave problems, which is of increasing importance with the prospect of moving to millimetre wave technologies for 5G wireless systems.

We confine ourselves in this discussion to the deterministic methods, i.e. those giving a unique solution given a well-posed problem subject to prescribed boundary and initial conditions. Common numerical methods include the Finite Difference Method (FDM) [32, 33, 36] the Finite Element Method (FEM) [6, 15, 28] and the Boundary Element Method [3, 4, 5]. Among these methods, the FEM is well established for dealing with complicated geometries or inhomogeneous media, and the other methods also offer certain advantages, but they all remain constrained in term of the problem size. This is

mainly due to the fact that the computational domain may be very large (electromagnetic waves often propagate in free space), so that the size of the analysis domain and of scattering objects can greatly exceed the wavelength, typically by multiple orders of magnitude [8, 35]. Since a certain number of degrees of freedom are required to capture the solution over each wavelength, such problems can result in a very large system of equations. This can render them completely intractable using conventional FEM, FDM and BEM methodologies. Different authors vary in their recommendations, but a typical rule of thumb suggests the use of ten degrees of freedom in each wavelength for linear elements. To illustrate the problem, engineers may seek to analyse the scattering of a radar wave by an aircraft. Even if the analysis domain is confined to a 100 m cube surrounding the aircraft, a finite element model would require at least 10^{12} degrees of freedom to model the scattering of a radar wave of 100 mm wavelength to engineering accuracy.

To overcome this limitation without compromising the accuracy, the Partition of Unity enrichment method was proposed in [21] for harmonic wave problems governed by the Helmholtz equation. The method consists of enriching the approximation space with oscillatory functions that have better approximation properties compared to the standard low order polynomials usually used in the FEM. The enrichment idea spawned a large body of literature including the work on the Partition of Unity Finite Element Method (PUFEM) [7, 18, 19, 22] and also similar enrichment techniques such as the Generalised Finite Element Method [30, 31] the Ultra-Weak Variational Formulation [14, 20] and the Discontinuous Enrichment Method [9, 16, 34]. The enrichment approach is also used in other methods such as the Boundary Element Method [25, 26, 27]. A recent survey on various enrichment approaches could be found in [12].

The enrichment functions used in the case of harmonic wave problems, as presented above, are in the form of plane waves or radial waves and are solutions of the partial differential equations (PDEs) governing the problems. This latter aspect, while useful, is not necessary for incorporating $a - priori$ knowledge of the solution behaviour in the approximating field. This inspired the use of intuitive field enrichment functions capable of capturing the solution behaviour while not necessarily being solutions of the problem PDE. Such enrichment was proposed for solving heat transfer problems in the time domain [23, 24, 29]. The temperature field was enriched with Gaussian functions capable of modelling the high temperature gradients and led to the use of coarse mesh grids, instead of the very fine meshes employed in standard FEM, and hence to considerable savings in the computational effort. In spite of the problem being time dependent, the enrichment functions are independent of time, which permits the re-use of a single system matrix for all time steps, resulting in even further computational saving. The success of this approach has motivated the current work in developing the field-enrichment technique to solve time-dependent wave problems. It is worth noting that an enriched model for wave propagation in one dimensional problems was presented in [17]. Recently this was extended into two-dimensional transient wave problems [10] where the solution field within each finite element is discretized with the usual Lagrangian functions and enriched with harmonic functions, each with a prescribed frequency. In the current work, the PUFEM is used for the first time to solve the wave equation in the time domain. In previous work on the PUFEM only time harmonic problems were considered when solving the equation in the frequency domain. Instead here we show that the method could also be used for solving non-time-harmonic problems in the time domain. The wave field solution is presented as a sum of a slowly varying term and a highly oscillatory part, which is expanded into a sum of plane waves propagating in multiple directions. However, unlike other enrichment technique [10] here the plane waves have a fixed frequency. The performance of this approach is assessed for different test wave models where exact solutions are available. The results are compared to those obtained by a polynomial based FEM and also to another enrichment approach where the proposed scheme provides better accuracy at a reduced computational cost.

The paper is organised as follows. In section 2 we introduce the considered problem. Then in section 3 we present the proposed PUFEM model, while in section 4 the model is validated on two numerical test cases with analytical solutions. We finish with some concluding remarks and recommendations for future work in section 5

2 Transverse electric mode of propagation

To describe the techniques used for enriched finite elements we consider a linear wave equation in two-dimensional domains. Hence, let $\Omega \subset \mathbb{R}^2$ be an open bounded domain with Lipschitz continuous boundary Γ and let $[0, T]$ be the time interval for the wave propagation. The boundary-value problem considered in the current study is defined as

$$\frac{\partial^2 E}{\partial t^2} - c^2 \nabla^2 E = f(t, \mathbf{x}), \qquad (t, \mathbf{x}) \in [0, T[\times \Omega, \tag{1a}$$

$$\frac{\partial E}{\partial \hat{\mathbf{v}}} + hE = g(t, \mathbf{x}), \qquad (t, \mathbf{x}) \in [0, T[\times \Gamma, \tag{1b}$$

$$E(0, \mathbf{x}) = E^0(\mathbf{x}), \qquad \mathbf{x} \in \Omega, \tag{1c}$$

$$\frac{\partial E}{\partial t}(0, \mathbf{x}) = V^0(\mathbf{x}), \qquad \mathbf{x} \in \Omega, \tag{1d}$$

where $\mathbf{x} = (x, y)^\top$ are the Cartesian coordinates, t is the time variable, $\hat{\mathbf{v}}$ the outward unit normal on Γ, c and h are constants, and E the magnitude of the transverse electric field in the direction perpendicular to the domain plane. In (1), $f(t, \mathbf{x})$ and $g(t, \mathbf{x})$ are respectively, prescribed source and boundary functions, $E^0(\mathbf{x})$ and $V^0(\mathbf{x})$ are given initial conditions. Note that the model (1) represents the basis of many linear electromagnetic and acoustic propagation problems. For instance, applied to separate components of the linear electromagnetic field, it can represent an accurate and efficient solution for a short pulse propagating over long distances.

The time integration of the system (1) can be carried out using any implicit scheme including Newmark methods to avoid the very small time steps that may be required in simulations for explicit time integration schemes. However, the proposed spatial enrichment is time independent and hence independent of the choice of the integration scheme. The spatial discretization is introduced after the temporal one to enable changing the temporal discretization independently on the enrichment approach presented here. Alternative integration schemes can also be found in [2, 11]. For simplicity in the presentation we consider the second-order central difference method. The latter is well known and details could be found in standard text books [1]. Thus, to integrate the equations (1) in time we divide the time interval into N subintervals $[t_n, t_{n+1}]$ with length $\Delta t = t_{n+1} - t_n$ for $n = 0, 1, \dots$. We use the notation W^n to denote the value of a generic function W at time t_n. Thus, given the solutions E^{n-1} and E^n at times t_{n-1} and t_n the solution at the next time step t_{n+1} is updated according to the semi-discrete equation

$$\frac{E^{n+1} - 2E^n + E^{n-1}}{\Delta t^2} - c^2 \nabla^2 E^{n+1} = f(t_{n+1}, \mathbf{x}), \qquad n = 0, 1, 2, \dots,$$

$$E^0(\mathbf{x}) = E^0(\mathbf{x}), \tag{2}$$

$$E^{-1}(\mathbf{x}) = E^0(\mathbf{x}) - \Delta t V^0(\mathbf{x}).$$

Note that to update the solution E^{n+1} in the semi-discrete formulation (2) one has to solve a linear system at each time step. The structure of this linear system is mainly dependent on the mesh used in the spatial discretization and the time step used in the time integration.

For the spatial discretization, we multiply the equation in (2) by a weighting function $\phi(\mathbf{x})$, and then integrate over Ω. Using the divergence theorem and using the boundary condition (1b) one obtains the following weak formulation of the problem (1)

$$\int_\Omega E^{n+1} \phi \, d\Omega + (c^2 \Delta t^2) \int_\Omega \nabla E^{n+1} \cdot \nabla \phi \, d\Omega + (c^2 \Delta t^2) \oint_\Gamma (hE^{n+1}) \phi \, d\Gamma =$$

$$\int_\Omega \left(2E^n - E^{n-1} + (\Delta t^2) f(t_{n+1}, \mathbf{x}) \right) \phi \, d\Omega + (c^2 \Delta t^2) \oint_\Gamma g(t_{n+1}, \mathbf{x}) \phi \, d\Gamma. \tag{3}$$

To solve the weak formulation (3) with the finite element method we discretize the spatial domain Ω into a set of finite elements $\mathcal{T}_i$ with the index i referring to the i-th element. The combination of all these elements forms our computational domain $\Omega_h = \cup_i \mathcal{T}_i$, with $\Omega_h \subseteq \Omega$. If $\mathcal{T}_i$ and $\mathcal{T}_j$ are two different elements of Ω_h, then $\mathcal{T}_i \cap \mathcal{T}_j$ is either a mesh point, or a common side, or the empty set. The conforming finite element space for the solution that we use is defined as

$$V_h = \left\{ E_h^{n+1}(\mathbf{x}) \in C^0(\Omega): \quad E_h^{n+1}(\mathbf{x})\Big|_{\mathcal{T}_i} \in \Psi(\mathcal{T}_i), \quad \forall \, \mathcal{T}_i \in \Omega_h \right\}, \tag{4}$$

with

$$\Psi(\mathcal{T}_i) = \left\{ \psi(\mathbf{x}): \quad \psi(\mathbf{x}) = \widehat{\psi} \circ Y_j^{-1}(\mathbf{x}), \quad \widehat{\psi} \in \Psi_m(\widehat{\mathcal{K}}_e) \right\},$$

where $\widehat{\psi}(\mathbf{x})$ is a basis function defined on the element $\mathcal{T}_i$ and $\Psi_m(\widehat{\mathcal{K}}_e)$ is the set of all basis functions defined on the reference element $\widehat{\mathcal{K}}_e$. Here, $Y_i(\mathbf{x}): \widehat{\mathcal{K}}_e \longrightarrow \mathcal{T}_i$ is an invertible one-to-one mapping. Next, the finite element solution to $E^{n+1}(\mathbf{x})$ can be formulated as

$$E_h^{n+1}(\mathbf{x}) = \sum_{j=1}^{N_d} E_j^{n+1} \mathcal{N}_j(\mathbf{x}), \tag{5}$$

where N_d is the number of solution mesh points in the partition Ω_h. The coefficients E_j^{n+1} are the corresponding nodal values of the functions $E_h^{n+1}(\mathbf{x})$. They are defined as $E_j^{n+1} = E_h^{n+1}(\mathbf{x}_j)$ where $\{\mathbf{x}_j\}_{j=1}^{N_d}$ are the set of solution mesh points in the partition Ω_h. In (5), $\{\mathcal{N}_j\}_{j=1}^{N_d}$ are the set of global nodal basis functions of V_h characterized by the property $\mathcal{N}_i(\mathbf{x}_j) = \delta_{ij}$ with δ_{ij} denoting the Kronecker symbol. We introduce $\{\mathbf{x}_1, \mathbf{x}_2, \ldots, \mathbf{x}_M\}$ as the set of M nodal points in the element $\mathcal{K}_j$. We also define $\{\phi_j\}_{j=1}^{M}$ as the set of element basis coefficients for $\mathcal{K}_j$ in V_h characterized by the property $\phi_i(\mathbf{x}_j) = \delta_{ij}$. Hereafter, unless otherwise stated, the subscripts h and j are used to refer to coefficients associated with the whole mesh Ω_h and a mesh element $\mathcal{K}_j$, respectively. Note that the set $\{\phi_j\}_{j=1}^{M}$ is a local restriction on the element $\mathcal{K}_j$ of the set of the global basis functions $\{\mathcal{N}_j\}_{j=1}^{M}$. The approximation space is then defined as

$$\widetilde{V}_h^0 = \mathrm{span} \left\{ \mathcal{N}_h, \quad E_h^{n+1} = \sum_{j=0}^{N_d} E_j^{n+1} \mathcal{N}_j \right\}.$$

It should be stressed that most existing finite element methods applied to the model problem (1) employ in their formulation Lagrangian polynomials for the basis functions $\mathcal{N}_j(\mathbf{x})$. Linear and quadratic shape functions have been widely used in the literature for the finite element solution of equations (1), see for example [28, 6].

3 Partition of unity enrichment

In many application in electromagnetic waves modelled using the equations (1) the solution is expected to be highly oscillatory and is often recovered over vast domains. In these situations, the numerical solution obtained by a conventional finite element method either develops spurious oscillations or it is affected by a large numerical diffusion. Spurious oscillations and excessive numerical diffusion often deteriorate the accuracy of the finite element solution, so the numerical solution may become physically unacceptable. For this reason, in most finite element methods, very fine meshes have to be used to resolve wave propagation in transient wave problems. In order to avoid the principal drawback of the conventional finite element methods (5), that is the requirement of very fine meshes, we incorporate enrichment functions into the finite element space. Indeed, using the partition of unity method [21] it is possible to enrich the solution space with basis functions that have better

approximation properties than the conventional polynomial basis functions. In the current study, we introduce a further approximation by stating that the nodal values E_i^{n+1} consist of two terms; a slowly varying term and a highly oscillatory term. The former term captures slow variations in the solution, possibly a constant, and the latter term captures the highly oscillatory variations of the solution. This yields the following enriched finite element solution

$$E_h^{n+1}(\mathbf{x}) = \sum_{i=1}^{M} \mathcal{N}_i \left(B_i^{n+1} + \sum_{q=1}^{Q-1} A_i^{q,n+1} \; e^{\mathrm{i}k\,(x\cos\alpha_q + y\sin\alpha_q)} \right), \tag{6}$$

where k is a constant wavenumber and i the imaginary number (i $= \sqrt{-1}$). Given the aim of this work, which is to validate the proposed enrichment model for time-dependent wave problems, the wavenumber of the enrichment functions is chosen to coincide with that of the exact solution. However, in practical applications usually involving wave scattering from physical bodies, the wavenumber of the enrichment functions should coincide with that of the impinging wave field [13]. The exponential term represents a plane wave propagating in the direction $(\cos\alpha_q, \sin\alpha_q)^\top$ with $\alpha_q = 2\pi\,q/(Q-1)$. The unknown variables are not the nodal values of the electric field any more but the amplitudes B_i^{n+1} and $A_i^{q,n+1}$ both given at the time step $n+1$ and node i. The amplitudes of $A_i^{q,n+1}$ are also given with respect to each direction α_q. For a standard FEM approach to the solution of expression (5) the elementary matrices are of dimension $M \times M$, whereas for the proposed model of expression (6) the size of the elementary matrices increases to $M_q \times M_q$ with $M_q = M \times Q$. However, the use of enrichment usually leads to coarse meshes, and hence smaller linear systems of equations to be solved.

Gauss–Legendre quadrature scheme is adopted for the evaluation of the integrals given by the weak form (3). Notice that in the case of the PUFEM the enrichment functions are integrated over multi-wavelength sized elements using a high number of integration points. This is important to accurately capture the oscillations within such elements. However, the computational costs remain moderate despite the large number of integration points within each element due to the relatively small total number of elements compared to the standard FEM. It is also worth remarking that the enrichment functions in (6) are written using the global coordinates $\mathbf{x}$, but they are multiplied by the nodal shape functions $\mathcal{N}_j$ which are expressed in the local coordinates. For a given element $\mathcal{T}_i$, the elementary matrix is reconstructed by blocks $\mathcal{A}_{ij}$ as

$$\begin{pmatrix} \mathcal{A}_{11} & \mathcal{A}_{12} & \dots & \mathcal{A}_{1M} \\ \mathcal{A}_{21} & \mathcal{A}_{22} & \dots & \mathcal{A}_{2M} \\ \vdots & \vdots & \ddots & \vdots \\ \mathcal{A}_{M1} & \mathcal{A}_{M2} & \dots & \mathcal{A}_{MM} \end{pmatrix} \begin{Bmatrix} \mathbf{E}_1 \\ \mathbf{E}_2 \\ \vdots \\ \mathbf{E}_M \end{Bmatrix} = \begin{Bmatrix} \mathbf{b}_1 \\ \mathbf{b}_2 \\ \vdots \\ \mathbf{b}_M \end{Bmatrix}, \tag{7}$$

where the unknown solution $\mathbf{E}_j$, the right-hand side $\mathbf{b}_j$ and the sub-matrices $\mathcal{A}_{ij}$ are blocks that are defined below. It should be pointed out that in the proposed finite element method, the enrichment functions are associated with nodal points in each element. Hence, each block matrix $\mathcal{A}_{ij}$ in the system (7) is associated with the nodes i and j whereas, the corresponding block vectors $\mathbf{E}_j$ and $\mathbf{b}_j$ are associated with the node j. It is also evident that the size of the elementary matrix and the associated vectors (7) vary depending on the number of the element nodes as well as the number of enrichment functions Q. The higher the number of element nodes or the higher Q is the larger the

size of the elementary matrix (7). The individual blocks $\mathcal{A}_{ij}$, $\mathbf{E}_j$ and $\mathbf{b}_j$ can be reformulated as

$$\mathcal{A}_{ij} = \begin{pmatrix} a_{ij}^{11} & a_{ij}^{12} & \cdots & a_{ij}^{1Q} \\ a_{ij}^{21} & a_{ij}^{22} & \cdots & a_{ij}^{2Q} \\ \vdots & \vdots & \ddots & \vdots \\ a_{ij}^{Q1} & a_{ij}^{Q2} & \cdots & a_{ij}^{QQ} \end{pmatrix}, \qquad \mathbf{E}_j = \begin{Bmatrix} B_j^{n+1} \\ A_j^{2,n+1} \\ \vdots \\ A_j^{Q,n+1} \end{Bmatrix}, \mathbf{b}_j = \begin{Bmatrix} b_j^1 \\ b_j^2 \\ \vdots \\ b_j^Q \end{Bmatrix},$$

Assuming that the nodes i and j are not on the domain boundary then entries of the above blocks can be written as

$$b_j^1 = \int_\Omega \Big(2E_j^n - E_j^{n-1} + \Delta t^2 f(t_{n+1}, \mathbf{x}) \Big) \mathcal{N}_j \, d\Omega,$$

$$b_j^2 = \int_\Omega \Big(2E_j^{2,n} - E_j^{2,n-1} + \Delta t^2 f(t_{n+1}, \mathbf{x}) \Big) \mathcal{N}_j e^{\mathrm{i}k\,(x\cos\alpha_2 + y\sin\alpha_2)} \, d\Omega$$

and

$$b_j^s = \int_\Omega \Big(2E_j^{s,n} - E_j^{s,n-1} + \Delta t^2 f(t_{n+1}, \mathbf{x}) \Big) \mathcal{N}_j e^{\mathrm{i}k\,(x\cos\alpha_s + y\sin\alpha_s)} \, d\Omega$$

with

$$a_{ij}^{11} = c^2 \Delta t^2 \int_\Omega \Big(\nabla \mathcal{N}_i \cdot \nabla \mathcal{N}_j + \mathcal{N}_i \mathcal{N}_j \Big) \, d\Omega,$$

$$a_{ij}^{22} = c^2 \Delta t^2 \int_\Omega \bigg(\nabla \Big(\mathcal{N}_i e^{\mathrm{i}k\,(x\cos\alpha_2 + y\sin\alpha_2)} \Big) \cdot \nabla \Big(\mathcal{N}_j e^{\mathrm{i}k\,(x\cos\alpha_2 + y\sin\alpha_2)} \Big)$$
$$+ \Big(\mathcal{N}_i e^{\mathrm{i}k\,(x\cos\alpha_2 + y\sin\alpha_2)} \Big) \Big(\mathcal{N}_j e^{\mathrm{i}k\,(x\cos\alpha_2 + y\sin\alpha_2)} \Big) \bigg) \, d\Omega$$

and

$$a_{ij}^{sq} = c^2 \Delta t^2 \int_\Omega \bigg(\nabla \Big(\mathcal{N}_i e^{\mathrm{i}k\,(x\cos\alpha_s + y\sin\alpha_s)} \Big) \cdot \nabla \Big(\mathcal{N}_j e^{\mathrm{i}k\,(x\cos\alpha_q + y\sin\alpha_q)} \Big)$$
$$+ \Big(\mathcal{N}_i e^{\mathrm{i}k\,(x\cos\alpha_s + y\sin\alpha_s)} \Big) \Big(\mathcal{N}_j e^{\mathrm{i}k\,(x\cos\alpha_q + y\sin\alpha_q)} \Big) \bigg) \, d\Omega$$

Assembling the elementary matrices, the numerical solution of the problem (1) is obtained by solving at each time step a linear system of the form

$$\mathbf{A}\mathbf{E}^{n+1} = \mathbf{b}, \tag{8}$$

where the system matrix $\mathbf{A}$ is symmetric and composed of the block matrices $\mathcal{A}_{ij}$ which are zero block matrices unless the nodes i and j belong to the same element. Note that similar to the standard finite element methods, the assembly process needs to consider the nodes shared between the elements. However, in the proposed enriched finite element method the overlapping part of the matrix includes an entire block matrix $\mathcal{A}_{ij}$ rather than a single entry.
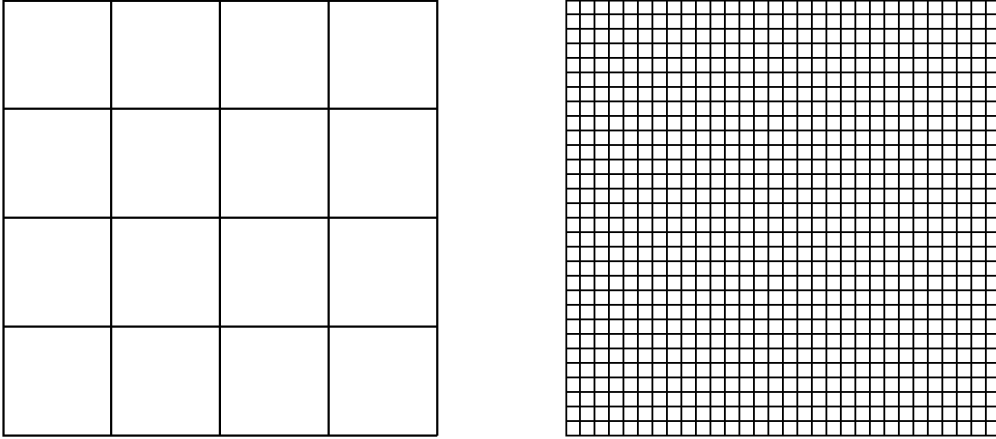
Figure 1: Mesh with 25 nodes used in the PUFEM mesh (left) and mesh with 961 nodes used in the FEM (right).

It is worth remarking that at each time step, the solution procedure automatically provides the amplitudes of the different enrichment functions used. In the current study, we factorize the matrix using an $\mathrm{LUL}^\top$ decomposition at the first time step; thus, the solution is reduced into backward/forward substitutions. This can significantly increase the efficiency when a large number of time steps is needed, compared to updating the matrix and fully solving the system at every time step. We note that the conventional finite element method also offers time independence, but the considerably greater system size may preclude us from computing, storing and re-using an $\mathrm{LUL}^\top$ decomposition.

4 Numerical tests

To evaluate the performance of the proposed partition of unity finite element method (PUFEM) we solve several numerical tests for transverse electromagnetic waves. We use models with known analytical solutions of the boundary-value problem (1) such that the error can be quantified. Here, the analytical solutions involved in the first test cases include a plane wave, waves with a varying wavenumber and a Hankel source then in the second case it is a progressive cylindrical wave while in the last case it is a wave front progressing inside a stationary domain. We calculate the relative error in $L^p(\Omega)$ as

$$\mathrm{Error} = \frac{\left\| E - \widetilde{E} \right\|_{\mathrm{L}^p(\Omega)}}{\left\| \widetilde{E} \right\|_{\mathrm{L}^p(\Omega)}},$$

where E is the numerical solution and $\widetilde{E}$ the analytical solution of the problem under study. The first test examples were taken from reference [10]. The performance of the approach presented here is compared to the approach used in [10]. For the last two test examples the numerical results obtained using the PUFEM are compared to those obtained using the conventional finite element method results. The CPU time is measured in seconds on a machine running Ubuntu 14.04 LTS (64 bit) with an Intel® Core™2 Quad CPU Q8300 @ 2.50GHz × 4 and 4GB of RAM.

4.1 Comparison with previous work

In our first set of results we aim to compare the performance of the PUFEM to a previous approach [10]. It should be noted that all the following problems are initialized at $t = 0.0$ and solved for a single iteration in time with the step size $\Delta t = 10^{-4}$.
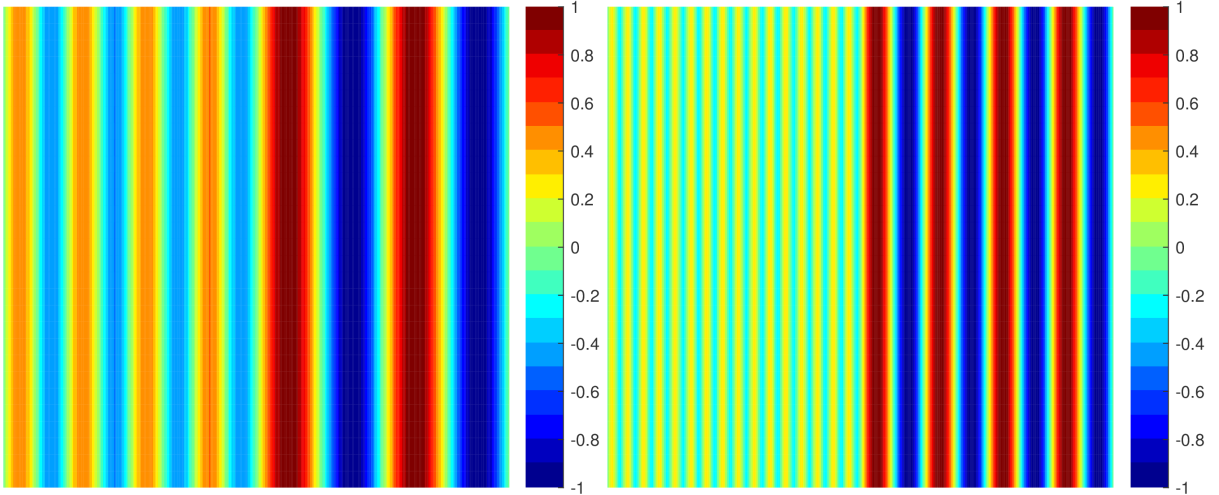
Figure 2: Comparison with previous work: PUFEM solution of the discontinuous k case 1 (left) and case 2 (right).

First we choose the progressive plane wave example proposed in [10] where the exact solution is given by $u(x, y) = A \sin(kx - \omega t)$. Here A is the wave amplitude and ω is the angular frequency. A constant wavenumber $k = 4\pi$ and a constant phase velocity $c = \frac{\omega}{k} = 1$ are also considered. The problem is solved over the spatial domain $[0, 1] \times [0, 1]$ which is discretized into a 4×4 uniform mesh of 4-noded linear elements as shown in Figure 1. Two plane waves with the same k as that of the problem and at the angles 0 and π, are used for enrichment together with the slowly varying term. Hence, the total number of degrees of freedom is 75. The solution L_2-norm error is $7.9 \times 10^{-5}\%$. The same problem is solved in [10] on a 10×10 uniform mesh of 4-noded elements and with the cutoff numbers $(2, 2)$ leading to 3025 degrees of freedom and an L_2-norm error of the order 1.0%. This confirms the efficiency of the PUFEM in solving this type of problems.

To compare the two approaches further we consider another test example that is also published in [10]. Again we consider the same exact solution as before but now A, k and ω may vary in space in a piecewise-constant fashion. The spatial domain is $[0, 2] \times [0, 2]$. In the reference the problem is solved for two cases. Each case involves different wavenumbers which are also considered here. In the first half of the domain $[0, 1] \times [0, 2]$ we have $A = 0.5, k = 8\pi$ and $\omega = 8\pi$ (case 1) and $A = 0.25, k = 32\pi$ and $\omega = 32\pi$ (case 2) while in the second half $[1, 2] \times [0, 2]$ we have $A = 1, k = 4\pi$ and $\omega = 4\pi$ (case 1) and $A = 1, k = 8\pi$ and $\omega = 8\pi$ (case 2). Compared to the previous test this is a more challenging problem due to the discontinuous parameters. The computational domain is discretized using 14 uniform 4-noded linear elements and a total of 30 nodes in case 1 and 24 uniform 4-noded linear elements and a total of 50 nodes in case 2. The same enrichment as before is also used where the enrichment wavenumbers at each node are chosen to match those of the problem at the same node. The total number of degrees of freedom is now 90 in case 1 and 150 in case 2. Figure 2 shows the numerical solution obtained with the PUFEM for both cases. Figure 3 shows at the cross section $(y = 0)$ the difference between the exact solution and the numerical solution using the PUFEM, compared to that of the solution in [10]. The results in [10] are obtained with enrichment and using linear elements and quadratic elements which are referred to as Ref1 and Ref2, respectively, in the figure. The results show that using similar numbers of degrees of freedom or even fewer, the PUFEM leads to about one order of magnitude smaller differences compared to the results in [10].

Obviously, the two previous test examples can be reduced into one-dimensional problems. To confirm that the PUFEM approach can also work for two-dimensional problems we again consider the second test example but with the exact solution now given as $u(x, y, t) = A \sin(kr - \omega t)$ where r is the distance from the point $(0.5, 0)$. The wave is now cylindrical while it was plane before. The amplitude A, wavenumber k and the angular frequency ω are now dependent on r such that for $0 \le r < 1.5$
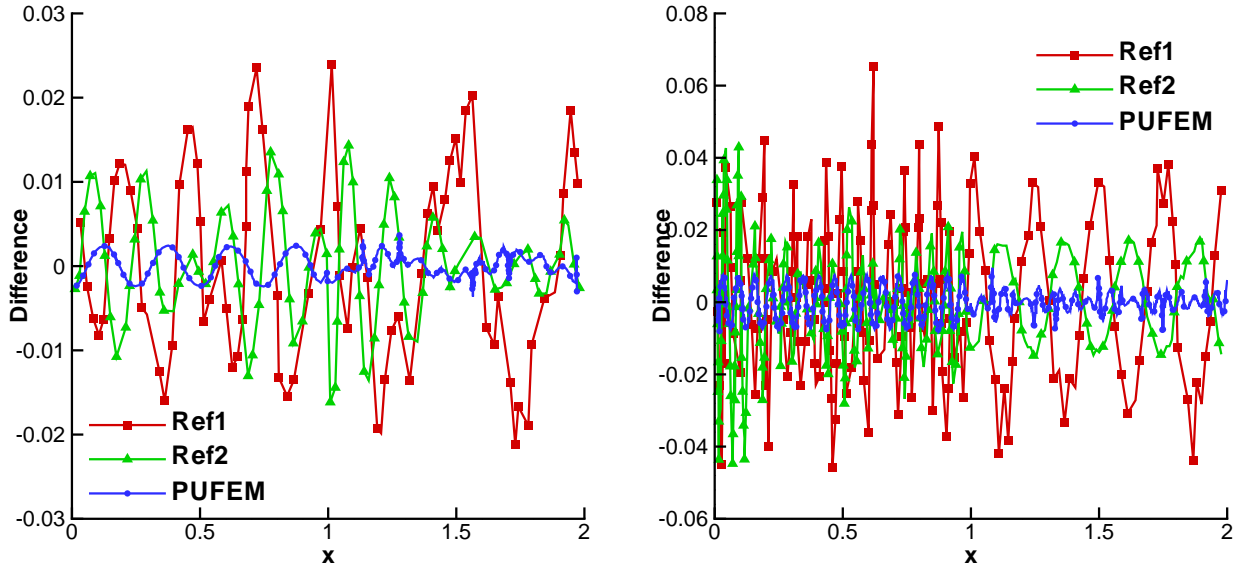
8

Figure 3: Comparison with previous work: absolute difference between the exact and the numerical solutions of the discontinuous k at $y = 0$ case 1 (left) and case 2 (right).

we have $A = 0.5$, $k = \omega = 8\pi$ and otherwise $A = 1$, $k = \omega = 4\pi$. The computational domain is bounded on the outside by the square $[-2.0, 2.0] \times [-2.0, 2.0]$ and on the inside by a unit circle centred at the origin. To solve the problem with the PUFEM the domain is meshed into eight 9-noded quadratic elements shown in Figure 4 with the total number of nodes being 48. The solution space is enriched with 27 functions including 26 evenly spaced plane waves. Again here the wavenumber of the enrichment functions at any node, is chosen to match the problem wave number at the same node. The total number of degrees of freedom in this case is 1296. Figure 4 shows the PUFEM solution of the problem where the achieved L_2-norm error in this case is 0.5%.

Finally, we consider the Hankel source test example that is also published in the same reference [10]. The exact solution of the problem is given by $u(x, y) = \mathrm{H}_0^{(1)}(kr)e^{-\mathrm{i}\omega t}$ where $r = \sqrt{(x - x_0)^2 + (y - y_0)^2}$ and $\mathrm{H}_0^{(1)}$ is the Hankel function of the first kind and order zero while $x_0 = 0.5$, $y_0 = 0$ and $k = \omega = 22$. The same computational domain and mesh as in the previous case are also considered here, however, now we use $Q = 25$. The PUFEM solution is shown in Figure 4 where the L_2-norm error is 0.2% and is achieved with 1200 degrees of freedom. The error achieved in the reference is about 4% using 9-noded elements with the total number of nodes being 576. The used cut-off number is $(2, 2)$ which leads to the total number of degrees of freedom 14400. Again the efficiency of the proposed approach can be clearly seen from the presented results.

4.2 Cylindrical progressive wave problem

In the second test example we consider the problem of recovering a progressive cylindrical wave in a unit squared domain. Here we solve the boundary-value problem (1) in $\Omega = [0.1, 1.1] \times [0.1, 1.1]$ subject to the initial conditions

$$U_0 = e^{\mathrm{i}kr},$$
$$V_0 = e^{\mathrm{i}kr}(-\mathrm{i}\omega),$$

where r is the length of the position vector. The source term $f(t, x, y)$ and the boundary $g(t, x, y)$ function in (1) are defined such that the analytical solution of this test problem is a progressive cylindrical wave given by

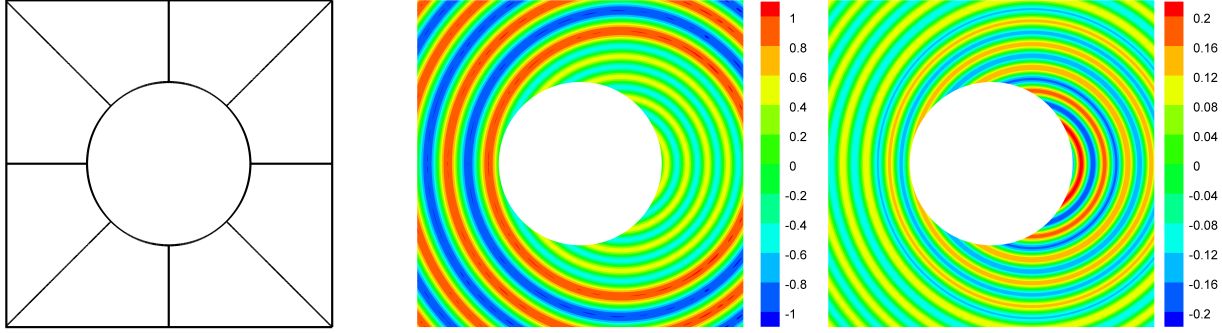$$\widetilde{E}(t, x, y) = e^{\mathrm{i}(kr - \omega t)}. \tag{9}$$

9

Figure 4: Comparison with previous work: Mesh (left) and the real part of the numerical solution for the cylindrical wave (middle) and the Hankel source (right).
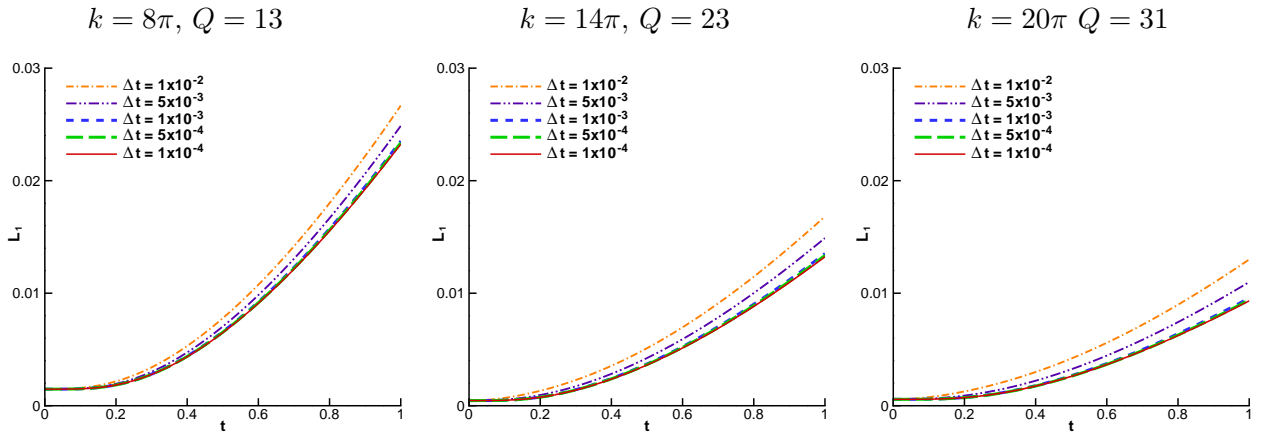

Figure 5: Cylindrical wave problem: the relative errors for different wavenumbers and different time step sizes.

Note that the function $g(t, x, y)$ is defined on each domain edge according to the relevant normal direction and the constant c in equation (1a) becomes the phase velocity.

4.2.1 Sensitivity of the results on time steps

Our first aim in this test example is to study the convergence of the proposed approach with respect to the time step size. Three wavenumbers are considered, namely $k = 8\pi$, 14π, and 20π with only one angular frequency $\omega = 1$. Therefore, the phase velocity c decreases with increasing the wavenumber. The number of wavelengths contained in the domain will increase from 4 with the smallest wavenumber to 10 with the highest wavenumber considered in our simulations. The problem is solved using the PUFEM on the coarse mesh of 16 uniform 4-noded linear elements shown in Figure 1. The solution space for the wavenumber $k = 8\pi$ is enriched with $Q = 13$. For the higher wavenumbers considered, the number of enrichment functions is increased to $Q = 23$ for $k = 14\pi$ and to $Q = 31$ for $k = 20\pi$. The wavenumber of the enrichment functions is chosen to be the same as the wavenumber of the exact solution. We consider five time steps in the simulation, $\Delta t = 1.0 \times 10^{-2}$, 5.0×10^{-3}, 1.0×10^{-3}, 5.0×10^{-4}, and 1.0×10^{-4}. The results for the cylindrical wave are presented in the time interval $[0, 1.0]$. It should be mentioned that using the same mesh and only changing the number of enrichment functions for different wavenumbers is a particularly useful feature of the proposed PUFEM. Otherwise using the standard FEM, increasing the values of wavenumbers requires refining the mesh.

The evolution of the relative error in time is plotted in Figure 5 for all the considered wavenumbers and time step sizes. For each wavenumber the figure shows that decreasing the time step Δt always
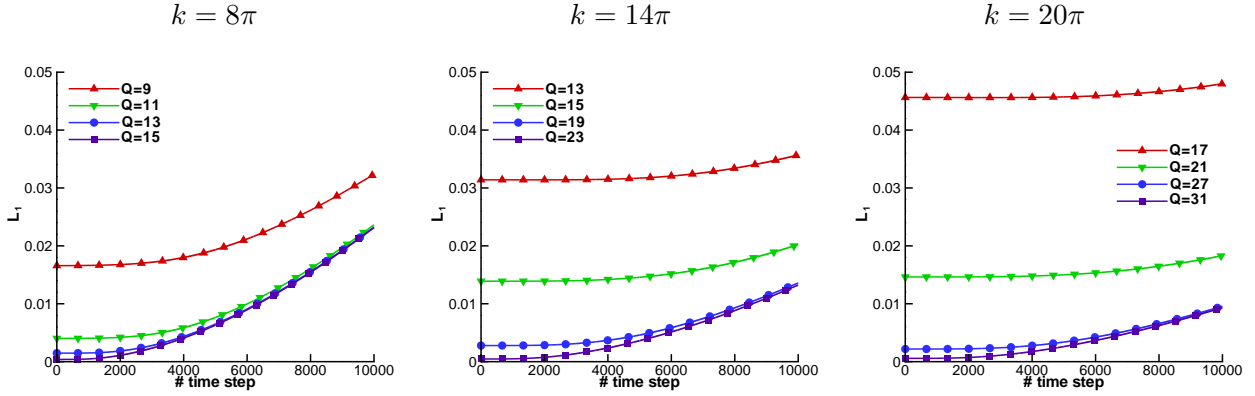
Figure 6: Cylindrical wave problem: relative errors obtained for the three considered wavenumbers and for different Q where $\Delta t = 1.0 \times 10^{-04}$.

reduces the relative error. At very small time steps this reduction in the error becomes insignificant. This can be seen with the relative errors for $\Delta t = 1.0 \times 10^{-3}$ and 5.0×10^{-4}, which are very close to each other, while those for $\Delta t = 5.0 \times 10^{-4}$ and 1.0×10^{-4} are almost identical. This is attributed to the fact that for small time steps the errors in the simulated solutions are dominated by the spatial discretization rather than the time integration procedure. Once the error in the numerical solution becomes dominated by the spatial error, refining Δt cannot further reduce the relative errors. The same behaviour is consistently observed for the three wavenumbers considered in our simulations. It also can be added that the proposed approach is similar to the standard FEM in that the convergence in time needs to be checked by considering a finer time step and rerunning the analysis. Once the error cannot be further reduced by refining the time step one may conclude that the solution has converged in time.

The results show that the proposed enrichment approach is stable as refining Δt reduces the relative errors in the obtained results. Another observation about this set of results is that for a given time step Δt, the accuracy of the numerical solution increases with a higher wavenumber. For example the maximum relative error with $k = 8\pi$ and for $\Delta t = 1.0 \times 10^{-2}$ is about 0.028 at time $t = 1$, while for the same Δt and at the same time $t = 1$ the error is about 0.012 for $k = 20\pi$. This is expected because for a higher wavenumber, the phase velocity $c = \frac{\omega}{k}$ becomes smaller. Hence, for a given time step Δt it is more accurate to capture a slower variation than a quicker one.

4.2.2 Sensitivity of the results on number of enrichments

Our next aim in this test example is to study the convergence of the proposed approach for an increased number of enriching plane waves. As mentioned earlier the use of at least ten degrees of freedom per wavelength is a requirement for the FEM to achieve engineering accuracy of about 1%. This number is reduced to about 2.5 degrees of freedom per wavelength or even less when using the PUFEM [18]. Here, the same wavenumbers and angular frequency are retained from the previous set of results. The problem is solved using the PUFEM on the previous mesh and using the time step size $\Delta t = 1.0 \times 10^{-4}$ as this leads to the lowest error in the previous set of results. The numbers of enrichment functions considered for $k = 8\pi$ are $Q = 9, 11, 13$ and 15. The numbers of enrichments for $k = 14\pi$ are $Q = 13$, 15, 19 and 23 while for $k = 20\pi$ we use $Q = 17, 21, 27$ and 31. The simulation is carried out for 10000 time steps.

As in the previous situation, we present in Figure 6 the evolution in time of the relative errors computed for each wavenumber. It is evident that adding more plane waves in the enriched finite element space improves the solution accuracy for all considered cases. This can be clearly seen in Figure 6 at the early time steps. As the simulation progresses in time the error accumulates faster with a higher Q and the difference between the errors obtained with different numbers of enrichment functions becomes
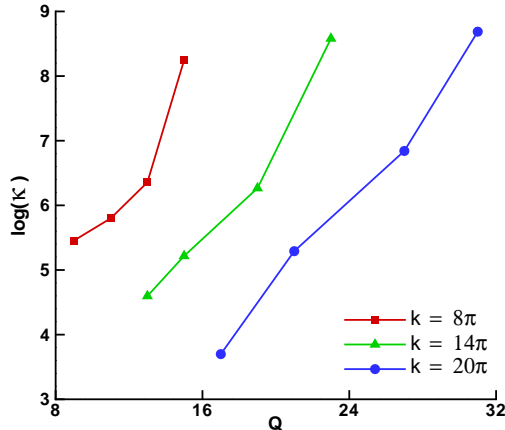
11

Figure 7: Cylindrical wave problem: conditioning of the linear system of equations resulting from the PUFEM for the cases shown in Figure 6 plotted against Q.

smaller. For example for $k = 8\pi$ after 4000 time steps the errors with $Q = 13$ and 15 become similar and then after 7000 time steps the errors with $Q = 11$, 13 and 15 become similar. For the considered wave conditions, as a higher wavenumber is considered in the simulations the accumulation of errors in time seems to become slower. However, for a given fixed wavenumber, a higher number of enrichment functions always accumulates errors faster.

It is also worth remarking in Figure 6 that for the same number of enrichment functions Q the relative error in the numerical solution accumulates faster for a lower wavenumber. For example, using $Q = 15$ with $k = 8\pi$ the relative error increases from less than 4×10^{-4} at the first time step to about 0.025 at the final time $t = 1$. However, for the same number of enrichment functions $Q = 15$ but with $k = 14\pi$ the relative error is 0.014 at the first time step and 0.020 at the end time $t = 1$. The relatively faster increase in the relative error at a lower wavenumber compared to a higher wavenumber may be attributed to the conditioning in the associated linear system that is well-known to affect the PUFEM; see for example [18, 22]. To further demonstrate this issue, we display in Figure 7 the condition numbers κ for the cases considered in Figure 6. These results show that for the same enrichment number Q a higher wavenumber always leads to a better conditioned linear system. The plots also reveal that for $k = 8\pi$, a condition number of order 10^8 is the outcome for the case with $Q = 15$ while the number of enrichment functions which produce a comparable condition number is $Q = 23$ for $k = 14\pi$ and $Q = 31$ for $k = 20\pi$. Hence, for a fixed mesh and a fixed condition number the number of enrichment functions can be increased when a higher k is considered. In fact the ratio between the element size and the wavelength determines the maximum number of enrichment functions that will lead to the ill-conditioning being controlled such that an accurate solution can be obtained. Having larger elements that span more wavelengths leads to better conditioned systems even with higher numbers of enrichment functions. For a better insight we also display in Figure 8 the imaginary parts of the numerical solutions obtained sing the PUFEM.

4.2.3 Comparison to the standard finite element method

Our final aim in this test problem is to compare the performance of the proposed approach to the standard FEM. The aspects compared include the number of degrees of freedom and the CPU time required to achieve a fixed relative error and the accumulation of relative errors in time. For this study we consider the test case with wavenumber $k = 6\pi$ and angular frequency $\omega = 1$ while we keep the time step fixed to $\Delta t = 1.0 \times 10^{-4}$ over the time interval $[0, 1]$. It should be noted that the selected wavenumber is relatively small because of the excessive computational cost required for the FEM to resolve this test problem, since a large number of time steps is considered to measure the accumulation
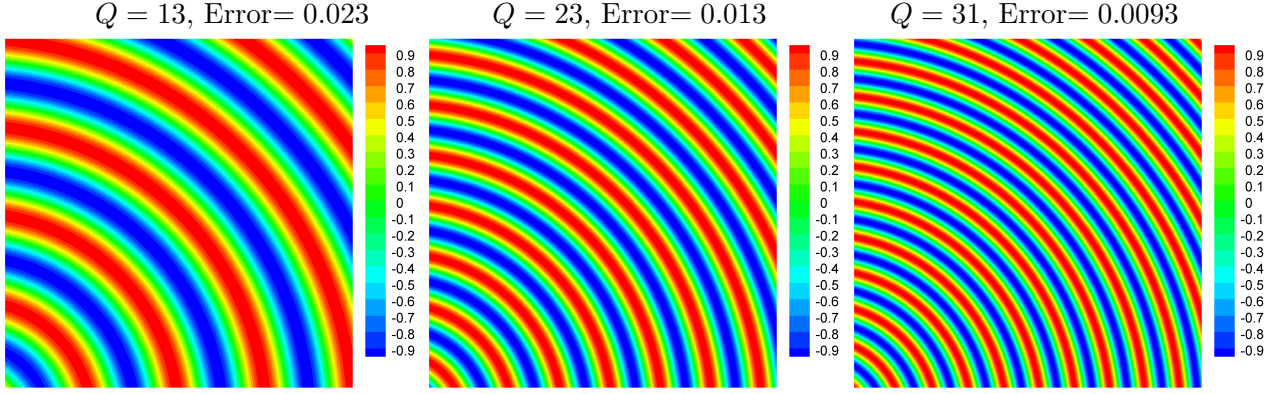
Figure 8: Cylindrical wave problem: imaginary part of the PUFEM solution at $t = 1.0$ for the wavenumbers $k = 8\pi, 14\pi$ and $k = 20\pi$ from left to right.
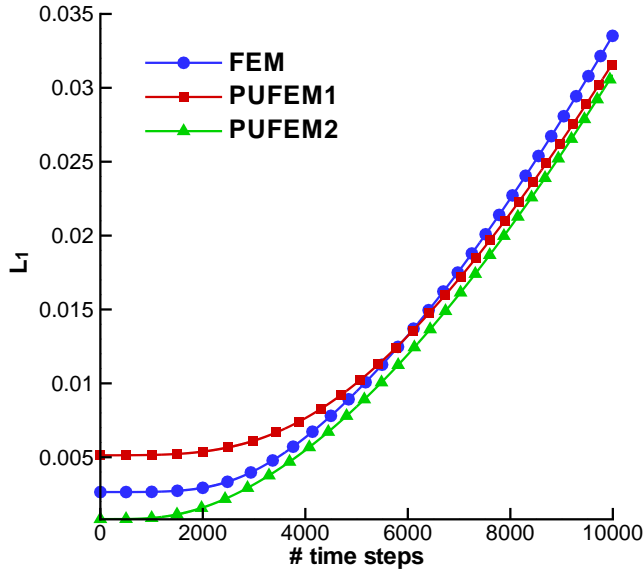

Figure 9: Cylindrical wave problem: relative error norms observed with the PUFEM and the FEM.

of errors in time.

The problem is first solved using the FEM on the fine mesh shown in Figure 1. The relative error achieved using the FEM at the first time step is about 0.0026 where the total number of degrees of freedom is $N_{dof} = 961$. Then the problem is solved using the PUFEM on the coarse mesh shown in Figure 1. Two different numbers of enrichment functions are considered, namely $Q = 9$ and $Q = 11$. The solution with the first enrichment number is referred to as PUFEM1 while the second as PUFEM2. The errors obtained at the first time step with PUFEM1 is 0.005 while with PUFEM2 it is 0.0008. The total numbers of degrees of freedom with the PUFEM1 and PUFEM2 are $N_{dof} = 225$ and $N_{dof} = 275$, respectively. In comparison to the FEM this is a reduction of about $77\% \sim 71\%$ in the required number of degrees of freedom to achieve a similar or even better relative error in this test problem. When using the FEM the CPU time needed to build the linear system of equations is 48.4s at the first time step. However, this time is reduced to 6.1s with PUFEM1 and 6.3s with PUFEM2. Starting from the second time step the FEM needs 37.7s to update the right hand side of the linear system while both PUFEM1 and PUFEM2 require less than 0.1s. To solve the linear system the CPU needs less than 0.1s in all the cases due to the relatively small system matrix.

Figure 9 illustrates the error accumulation in time for the FEM compared to the PUFEM1 and the PUFEM2. The plot shows that the accumulation of the relative error is faster using the FEM

13

compared to the PUFEM1. Note that the PUFEM1 starts from a higher error than the FEM, however at about 6000 time steps the relative error using the FEM and the PUFEM1 becomes equal to 0.0132. Thereafter the relative error using the PUFEM1 becomes better than that obtained using the FEM. The relative errors obtained using the PUFEM2 remain consistently lower than those with the FEM and the PUFEM1. At the end of the simulation after 10000 time steps, the relative errors obtained using the FEM, the PUFEM1 and the PUFEM2 are 0.034, 0.032 and 0.031, respectively.

To compare the number of degrees of freedom we calculate the number of degrees of freedom per wavelength $\tau = \lambda\sqrt{N_{dof}}$. For an acceptable engineering accuracy, a rule of thumb is to use at least ten degrees of freedom per wavelength when solving similar wave problems with the FEM. The number we used here is $\tau \approx 10.33$. On the other hand for the PUFEM and in order to achieve a similar or a better accuracy $\tau \approx 5$ is enough in this set of results. In fact in the previous set of results where wavenumbers higher than $k = 6\pi$ are considered, $\tau = 2.5$ is sufficient to obtain reasonable engineering accuracy in this test example. For instance, in the first set of results for $k = 20\pi$ and $Q = 31$ an accuracy better than 1% was achieved with $\tau \approx 2.7$. This shows the potential of the proposed approach for solving transient wave problems.

As a final comment we should mention that the effect of eliminating the slowly varying part of the enrichment (6) referred to by B_i^{n+1}, has an insignificant effect on the accuracy of the results in this test example. All the simulations presented in the current study were also repeated with the term B_i^{n+1} having been eliminated from the equation (6). This elimination has not changed the results, and this is expected because the solution varies quickly throughout the computational domain. The slowly varying term does not contribute to the numerical solution of this wave problem. However, our second test example provides an alternative platform to study the effect of including the slowly varying terms in the enrichment (6). It should be stressed that when B_i^{n+1} is eliminated the directions of the plane waves vary according to $\alpha_q = 2\pi q/Q$ and not $\alpha_q = 2\pi q/(Q-1)$ as before, such that the nodal degrees of freedom are expanded into plane waves only.

4.3   Moving envelope problem

In this section we consider the problem of a moving envelope governed by the transient wave problem (1). The source and boundary functions in (1) are defined such that the exact solution of this problem is given by

$$\widetilde{E}(t,x,y) = Ae^{iwf_L(t,x,y)}, \tag{10}$$

where $f_L(t,x,y)$ is the propagator function which provides a means to control the initial condition of the problem and can be used to manipulate the envelope of the moving wave such that the solution is a wave expanding symmetrically about the origin with evolution in time. In this example we examine the performance of the proposed PUFEM for this test example using two types of propagators F_1 and F_2 described in detail in Appendix A and Appendix B, respectively. Here, the propagator function F_1 behaves like a signum function and hence exhibits a sudden peak at the start of the envelope due to its discontinuous derivative as shown in Appendix A, whereas the other function F_2 has a continuous derivative and provides a smoother transition slope, which can be seen in Appendix B.

The computational domain in this test case is also considered to be a unit square and two wavenumbers $k = 4\pi$ and 8π are considered in our simulations. The time step and the angular frequency are $\Delta t = 1.0 \times 10^{-2}$ and $\omega = 1$, respectively. The domain is placed such that the wave will only enter after a time period equivalent to 100 time steps. The wave is initiated at the centre of the coordinate system, hence, the domain is defined by $\Omega = [c \times 100\Delta t, c \times 100\Delta t + 1] \times [c \times 100\Delta t, c \times 100\Delta t + 1]$. The considered time span starts from the wave entrance into the domain until the oscillations cover the entire computational domain. The problem is initialized with E^0 and V^0 which are obtained from the analytical solution (10) and its derivative at time $t = 0$. As in the previous test example, we use the weak form (3) and solve for the amplitudes.
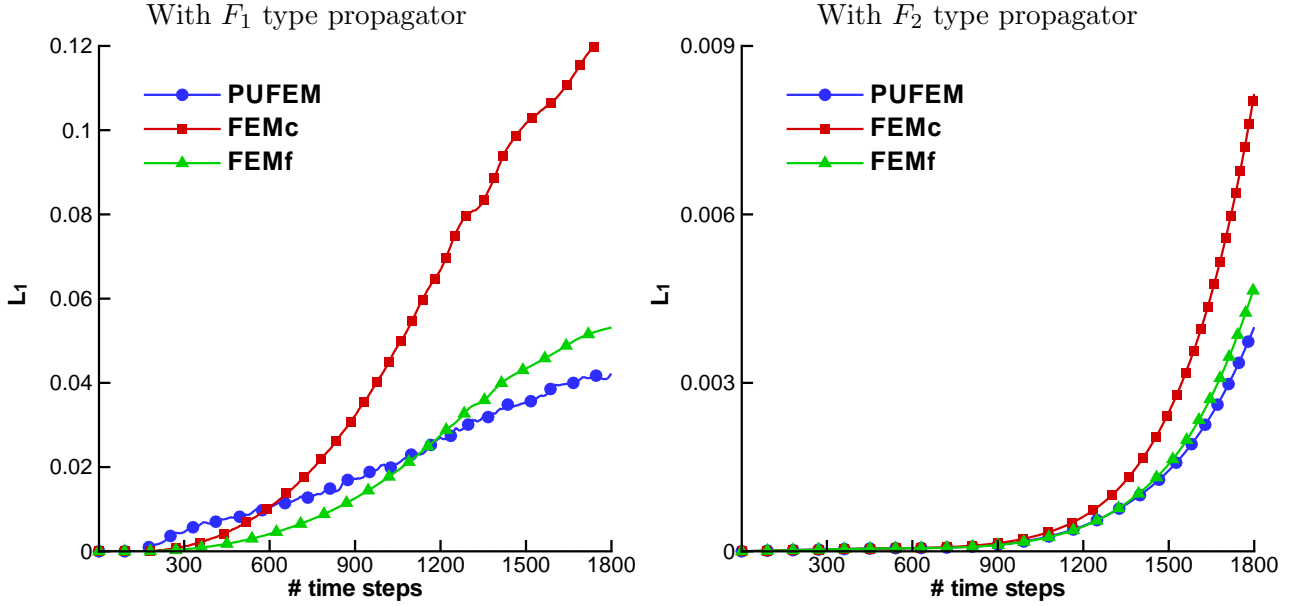
Figure 10: Moving envelope problem: comparison of the PUFEM with $Q = 11$ and the FEM on different meshes for the two types of propagators and for $k = 4\pi$

4.3.1 Discontinuity in time

The first aim in this example is to compare the proposed PUFEM to the standard FEM when recovering the solution with and without a discontinuity in time. The analytical solution with the F_1 propagator is used to measure the relative errors for the discontinuous case while the F_2 propagator is used for the continuous case. We solve the problem for $k = 4\pi$ using the PUFEM with $Q = 11$ on the coarse uniform mesh shown in Figure 1. In this situation, the total number of degrees of freedom is $N_{dof} = 275$. The wavenumber of the exact solution is also considered for the enrichment. The problem is then solved again using the FEM on two meshes. The first mesh, referred to as FEMc, is relatively coarse and composed of 361 uniform linear elements and 400 nodes. The second mesh is referred to as FEMf and is a fine mesh composed of 1521 elements and 1600 nodes. The obtained results are depicted in the time interval $[0, 18]$.

Figure 10 shows the evolution of the relative errors for both propagators F_1 and F_2 using the FEM on the two meshes as well as the PUFEM. The results using the F_1 propagator illustrate a relatively rapid increase in the relative error for both the FEM and the PUFEM. At earlier time steps the relative error increases faster in time for the PUFEM than for the FEM, hence, at $t = 4.0$ the results obtained using the PUFEM exhibit an error of about 0.006 while errors in the results obtained using the FEMc and the FEMf are 0.003 and 0.001, respectively. Thereafter the accumulation of the relative error in time becomes faster with the FEM such that at about $t = 6.0$ the error with the PUFEM (0.010) becomes slightly smaller than with the FEMc (0.011). Later at about $t = 11.5$ the PUFEM error (0.024) also becomes smaller than the FEMf error (0.025). At the end of the considered time span the errors with the PUFEM, the FEMc and the FEMf become $0.042, 0.124$ and 0.053, respectively.

On the other hand the results using the F_2 propagator show a gradual increase in the relative error compared to the discontinuous case. The final error with both methods remains below 1% at $t = 18$. Therefore one may conclude that the high values of relative errors in the previous case are mainly due to the discontinuous gradient, hence, having the second type propagator F_2 significantly improved the numerical results. Using the F_2 propagator and up to $t = 8$ the relative error seems to be unchanged using the FEM on either mesh or using the PUFEM. Thereafter the relative error starts to increase more rapidly using the FEMc compared to the FEMf and the PUFEM. Then at about $t = 15$ the relative error increases more rapidly using the FEMf than the PUFEM such that at the end of the
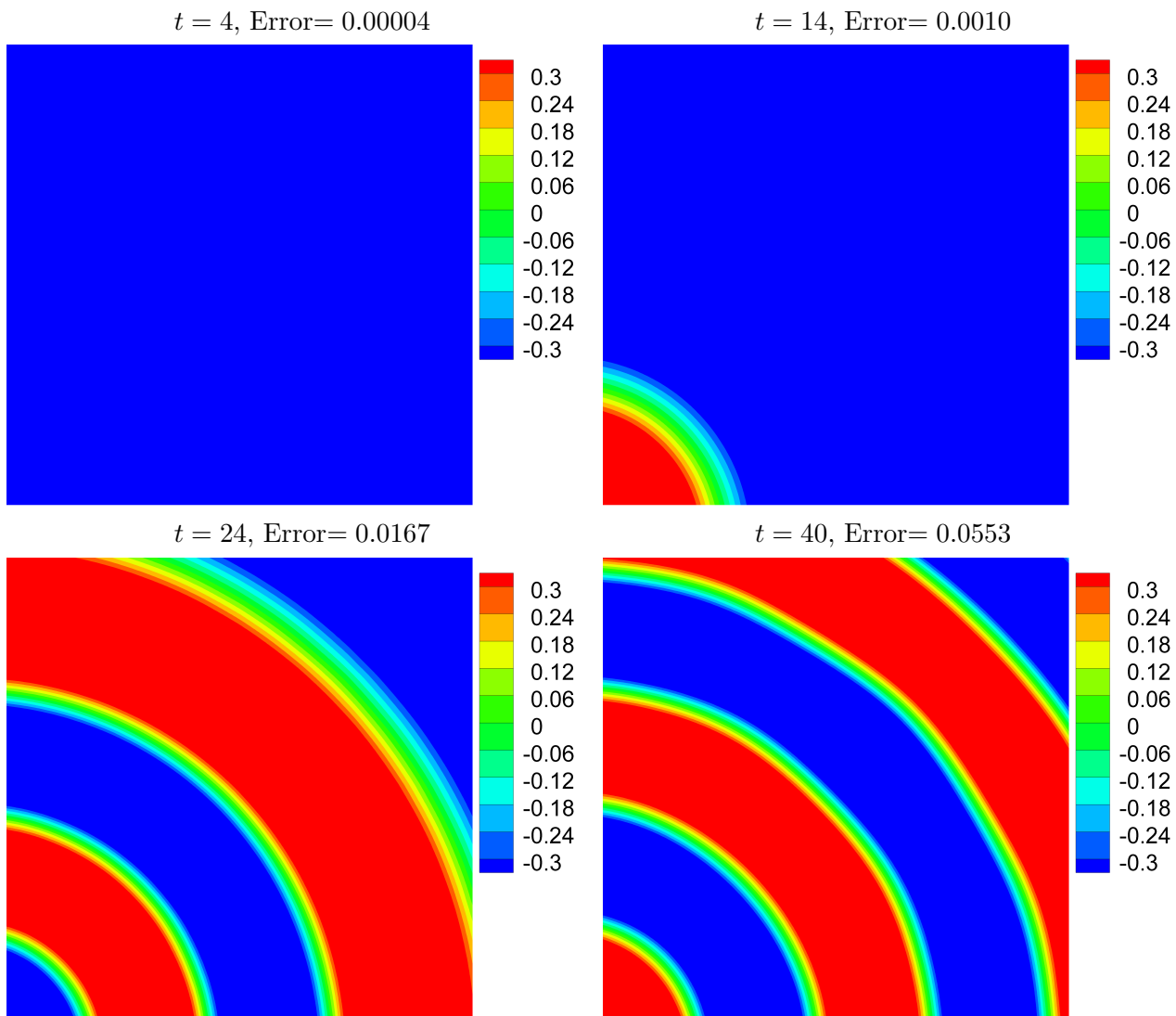
15

Figure 11: Moving Envelope problem: imaginary part of the PUFEM solution at different time instances for $k = 4\pi$, $Q = 11$, F_2 propagator and $\Delta t = 10^{-2}$
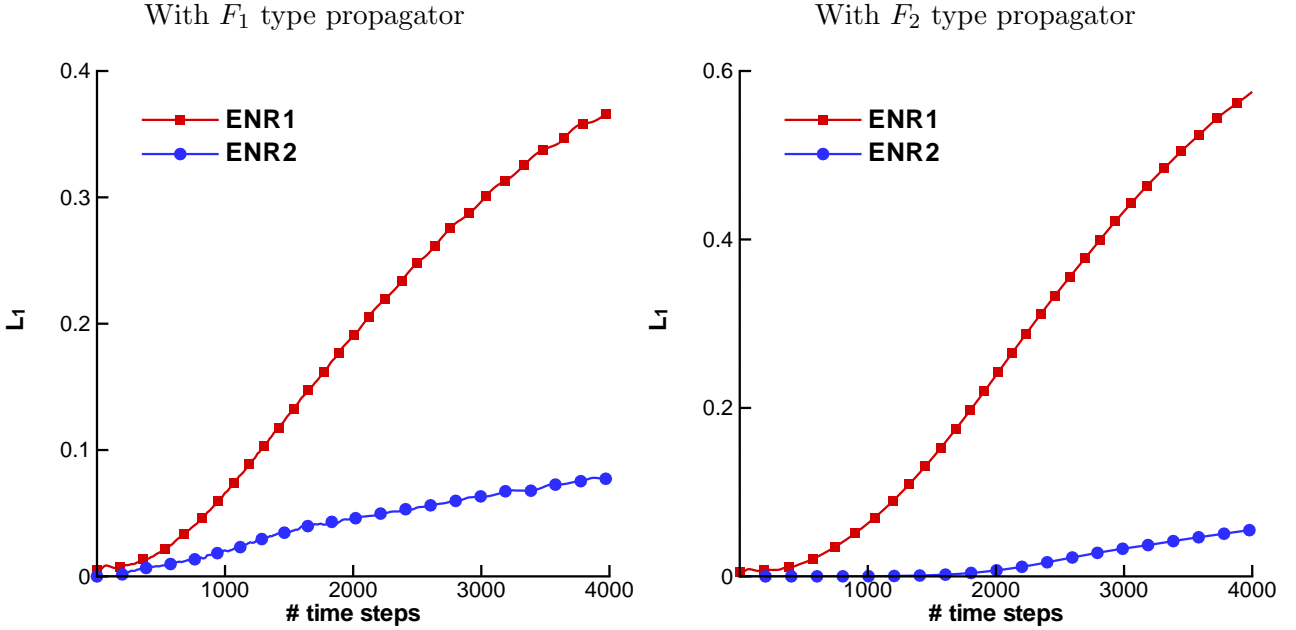
Figure 12: Moving Envelope problem: comparison of the PUFEM solution with $Q = 12$ (ENR1) and $Q = 11$ (ENR2) for $k = 4\pi$

simulation the values of the relative error obtained using the PUFEM, the FEMc and the FEMf become 0.0041, 0.0082 and 0.0047, respectively.

The results in Figure 10 reveal a consistent behaviour of the relative error which, up to a certain point in time, remains similar to the errors obtained using the FEM and the PUFEM with some advantage for the FEM as can be seen from the results obtained using the F_1 in Figure 10. Then the relative error starts to build up quickly using the FEM but becomes smaller with the PUFEM. This behaviour is mainly attributed to the propagation structure of the wave into the computational domain. Figure 11 presents snapshots of the numerical solutions obtained using the PUFEM at three different instants corresponding to the initial time, the phase when the wave progresses into the domain and until the domain is fully covered with oscillations. At the first few time steps the domain is mainly stationary and the solution is merely constant. The linear finite element can be very efficient in recovering such a constant solution. However, as the time passes, the oscillations start to cover a wider area of the computational domain while a smaller area remains stationary. It is clear that the PUFEM is much more efficient than the FEM in recovering such oscillations. Thus, the error starts to build up at a high rate with the FEM. Eventually, the relative errors obtained using the FEM tend to become larger than those obtained using the PUFEM.

4.3.2 Slowly varying enrichment term

Next we investigate the effect of the constant solution on the accuracy of the PUFEM. To achieve this we study the outcome of eliminating the slowly varying term B_i^{n+1} in the enrichment function from equation (6). The problem is solved again for $k = 4\pi$ using the PUFEM with 12 plane waves but without including the terms B_i^{n+1} in the enrichment. The computed solution is then compared to the solution obtained using the previous PUFEM where we have $Q = 11$, *i.e.* ten plane waves with the term B_i^{n+1} are included in the enrichment. All the problem parameters are retained but a longer time interval $[0, 40]$ is considered in this study. In Figure 12 we present a comparison of the relative errors between the results obtained using the PUFEM without B_i^{n+1} (referred to as ENR1 in the plots) and those obtained using the terms B_i^{n+1} (referred to as ENR2 in the plots). Although a larger number of enrichment functions is used for ENR1, the relative error for ENR2 is much smaller than for ENR1.
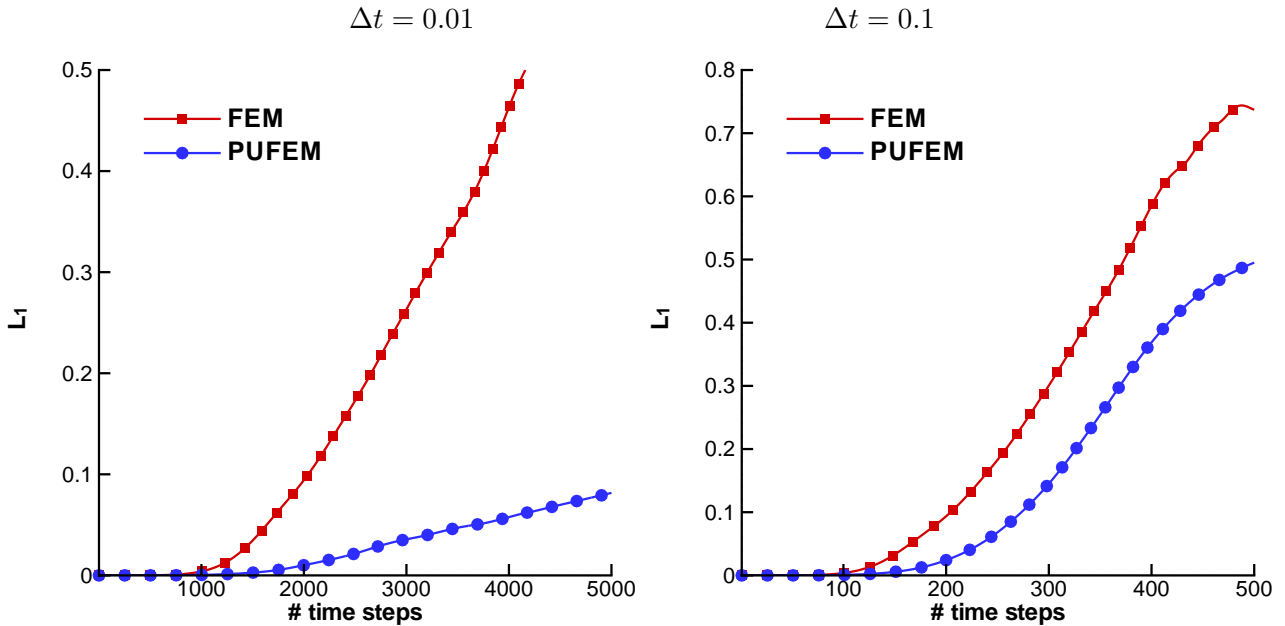
17

Figure 13: Moving Envelope problem: comparison of the results from PUFEM and FEM for $k = 8\pi$ with F_2 type propagator and $Q = 13$. The step size in time Δt is depicted under the plots.

Clearly the PUFEM does not produce useful results when B_i^{n+1} is eliminated and the relative error quickly increases to more than 10 %. Obviously removing the slowly varying terms B_i^{n+1} from the enrichment makes the PUFEM less efficient in capturing the stationary part of the numerical solution in this test example. The significant increase in the relative errors deteriorates the overall accuracy of the PUFEM applied to such waves problem in time domain.

4.3.3 Error accumulation in time

Finally, we evaluate the accumulation in time of the relative error for the enriched finite elements compared to non-enriched finite elements. To this end we solve the problem using the PUFEM and the FEM for $k = 8\pi$ and with the F_2 type propagator. For the PUFEM solution, the same mesh is retained from previous simulations but with $Q = 13$ such that $N_{dof} = 325$. For the FEM a mesh refinement is considered where the new mesh consists of 3481 uniform 4-noded linear elements and 3600 nodes. Note that such a fine mesh is necessary for the FEM in order to fulfil the ten degrees of freedom requirement for the high wavenumber considered in this case. The accumulation of the relative errors in time is summarized in Figure 13 using both methods and for two different time steps, namely $\Delta t = 0.1$ and 0.01. The time interval considered is $[0, 50]$.

Despite the much lower number of degrees of freedom with the PUFEM, it is clear that the error accumulates much more slow in time compared to the FEM. For $\Delta t = 0.01$ the FEM error reaches 0.1 at about $t = 20$ and it becomes 0.5 at about $t = 40$. On the other hand the PUFEM error does not exceed 0.08 for the entire time domain. Similar observations can also be made for the FEM and the PUFEM performance with $\Delta t = 0.1$. Figure 13 shows how the FEM error increases quickly with $\Delta t = 0.1$, and reaches Error= 0.1 at $t = 20.1$ and Error= 0.5 at about $t = 37.0$ while the PUFEM error reaches Error= 0.1 at $t = 27.0$ and 0.5 at the end of the simulation. When comparing the CPU time at the first time step the FEM requires 164.1s to solve the problem while the PUFEM requires 8.5s. At subsequent time steps this number is reduced to 147.7s with the FEM while it is only 1.3s with the PUFEM. Figure 14 shows snapshots of the PUFEM solution at several stages of the considered time span. The results and concluding remarks are consistent with those of the previous example.
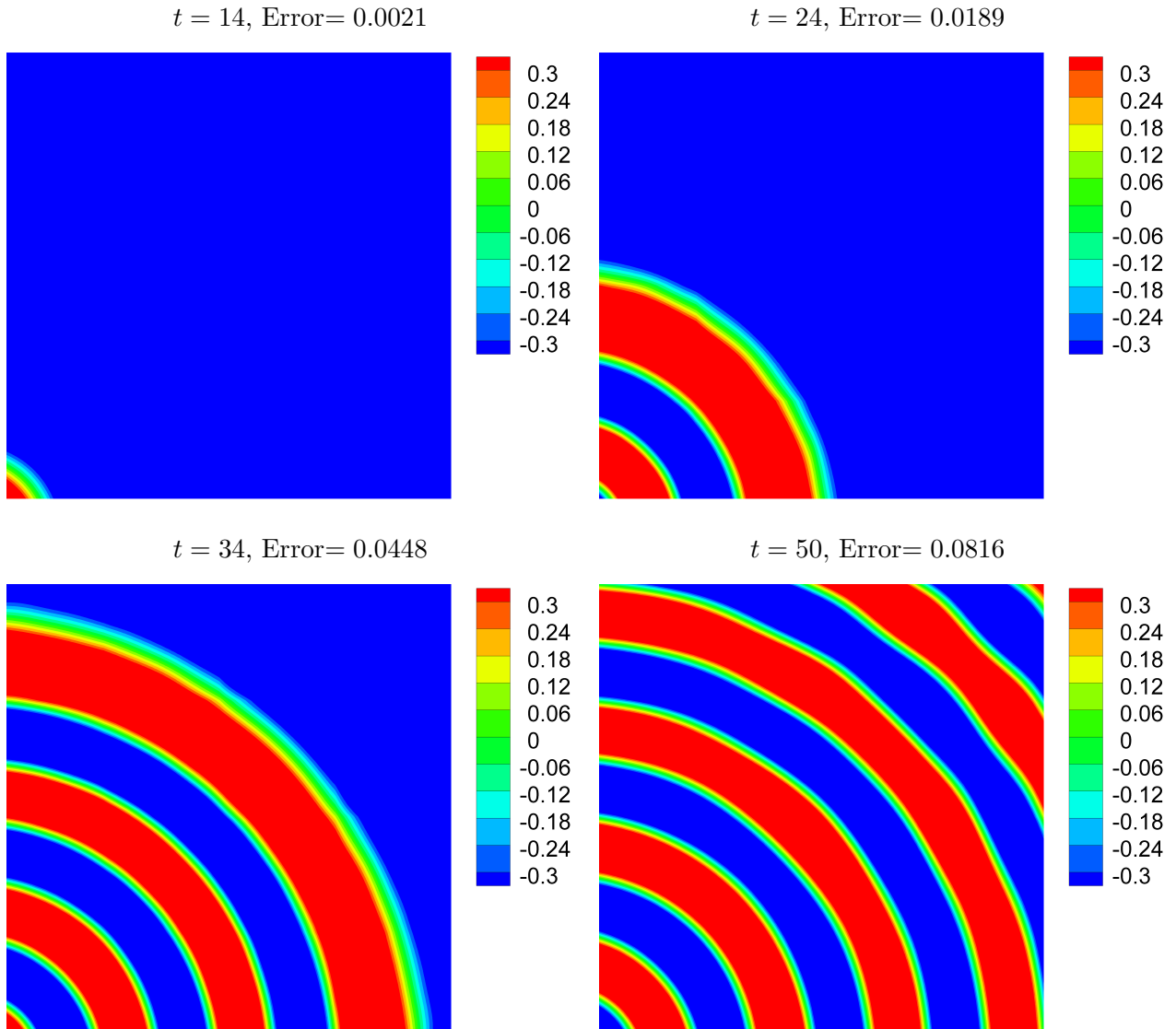
Figure 14: Moving Envelope problem: imaginary part of the recovered wave ($k = 8\pi$) with the propagator F_2, obtained using the proposed PUFEM with $Q = 13$, and $\Delta t = 10^{-2}$.

5 Conclusions

A class of enriched finite elements has been presented for solving the electromagnetic wave equation in the time domain. An implicit time integration procedure has been used to advance the numerical solution in the time domain. Using ideas from the partition of unity the finite element solution is enriched using plane wave functions. These techniques significantly reduce the number of degrees of freedom required for a fixed accuracy in the obtained solution compared to those needed for another enriched finite element method.

The performance of the proposed enriched finite element method is assessed for several test examples. First, the method is assessed by comparing its results to another enrichment technique where a number of publish test cases are considered. Next the performance of the method is assessed in two cases, namely a progressive cylindrical wave and a moving envelope, where the exact solutions are known. The accuracy of the proposed approach has been verified using the relative errors at different time steps and different numbers of enrichment functions. Comparison to the standard finite element method has also been presented. The numerical results confirm the accuracy of the proposed enriched finite element method and its performance for transient wave problems.

The results show that the partition of unity finite element method has the advantage of requiring less computational resources for the time-dependent wave problems compared to another enriched finite element method. This fact, as well as its favourable stability properties, make it an attractive alternative for solvers based on finite element techniques for the electromagnetic wave equation in the time domain where the considered problem involves few dominant frequencies. Future work will focus on developing other enrichment functions to deal with a wide spectrum of frequencies. It is also worthwhile to remark that the time integration scheme can be easily changed according to the transient wave problem under consideration. The advantages achieved with the enrichment approach can be further enhanced by considering a more efficient time integration scheme. Extension of the proposed enriched finite element method to three space dimensions is of particular interest as it will result in an extensive reduction in the computational resources compared to the classical methods. Furthermore, developing highly efficient solvers for the associated linear systems in order to resolve issues related to the conditioning and also developing efficient analytical integration procedures can further enhance the method.

A   Definition of the propagator $\mathbf{F}_1$

We consider a piecewise linear function given as

$$f_L(p) = \frac{p + |p|}{2}, \tag{11}$$

which is a continuous function but not differentiable at $p = 0$. The derivative of this function is given by

$$f_L'(p) = \frac{d\, f_L(p)}{d\, p} = \frac{f_L(p)}{|p|}, \qquad \text{with} \quad p \neq 0.$$

Thus, the derivative of the function is undefined for $p = 0$. Similarly for higher order derivatives $o \geq 2$ one obtains

$$\frac{d^o\, f_L}{d\, p^o} = 0, \qquad \text{with} \quad p \neq 0.$$

Note that

$$\left(f_L'(p)\right)^o = f_L'(p) = \frac{f_L(p)}{|p|}, \qquad \text{for} \quad o \geq 1.$$

In the current study, the independent variable p is chosen to be $t - \frac{r}{c}$ where t is time, r is the magnitude of the radial position vector $r = \sqrt{x^2 + y^2}$ and c is the speed of wave. Thus the propagator function

is denoted as follows

$$f_L(t, x, y) = \frac{t - \frac{r}{c} + |t - \frac{r}{c}|}{2}$$

This selection would facilitate to model the problem as a radially expanding wave centred at the origin (*i.e.* at $r = t = 0$).

B Definition of the propagator F_2

The propagator F_1 defined above is not well behaved around the origin. To overcome this drawback we define the propagator F_2 which resolves this problem and retains all the desired properties of the propagator F_1. In addition, the propagator F_2 promotes implementation of a radially evolving wave centred at $r = t = 0$. Hence, the function $f_L(p)$ in (11) is replaced by

$$f_L(p) = \frac{1}{1+a} \left(\text{erf} \left(\frac{p - p_0}{b} \right) (p - p_0) + ap + \frac{b}{\sqrt{\pi}} e^{-\frac{(p - p_0)^2}{b^2}} \right), \tag{12}$$

where $\text{erf}(\cdot)$ denotes the error function and p_0 is used to shift it towards the left or the right side of the origin. The parameters a and b are fixed to control the smoothness of the slope of the function near the origin. In the simulations reported in this study we use $a = 1$, $b = 5$ and $p_0 = 10$. The derivative of the function $f_L(p)$ in (12) is given by

$$\frac{d\, f_L(p)}{d\, p} = \frac{\text{erf} \left(\frac{p - p_0}{b} \right) + a}{1 + a}.$$

Thus, the derivative of the function $f_L(p)$ in (12) is a shifted and normalised error function which is well behaved. We used the following notation for the function $f_L(p)$

$$f_L(t, x, y) = \frac{1}{1+a} \left(\text{erf} \left(\frac{t - \frac{r}{c} - p_0}{b} \right) (t - \frac{r}{c} - p_0) + a(t - \frac{r}{c}) + \frac{b}{\sqrt{\pi}} e^{-\frac{(t - \frac{r}{c} - p_0)^2}{b^2}} \right)$$

References

[1] K J Bathe. *Finite Element Procedures*. New Jersey, 1996.

[2] K J Bathe. Frontiers in finite element procedures & applications. In B H V Topping and P Ivànyi, editors, *Computational Methods for Engineering Technology*, Stirlingshire, Scotland, 2014. Saxe-Coburg Publications.

[3] A Buffa, M Costabel, and C Schwab. Boundary element methods for Maxwell's equations on non-smooth domains. *Numerische Mathematik*, 92(4):679–710, 2002.

[4] A Buffa and R Hiptmair. Galerkin boundary element methods for electromagnetic scattering. In *Topics in computational wave propagation*, pages 83–124. Springer, 2003.

[5] A Buffa, R Hiptmair, T Petersdorff, and C Schwab. Boundary element methods for Maxwell transmission problems in Lipschitz domains. *Numerische Mathematik*, 95(3):459–485, 2003.

[6] D B Davidson. *Computational Electromagnetics For RF And Microwave Engineering*. Cambridge University Press, New York, 2011.

[7] G C Diwan, M S Mohamed, M Seaid, J Trevelyan, and O Laghrouche. Mixed enrichment for the finite element method in heterogeneous media. *International Journal for Numerical Methods in Engineering*, 101(1):54–78, 2015.

[8] J M Dlugach, M I Mishchenko, L Liu, and D W Mackowski. Numerically exact computer simulations of light scattering by densely packed, random particulate media. *Journal of Quantitative Spectroscopy and Radiative Transfer*, 112(13):2068 – 2078, 2011.

[9] C Farhat, I Harari, and U Hetmaniuk. A discontinuous Galerkin method with lagrange multipliers for the solution of Helmholtz problems in the mid-frequency regime. *Computer Methods in Applied Mechanics and Engineering*, 192(1112):1389 – 1419, 2003.

[10] S Ham and K J Bathe. A finite element method enriched for wave propagation problems. *Computers and Structures*, 9495(0):1 – 12, 2012.

[11] S Ham, B Lai, and K J Bathe. The method of finite spheres for wave propagation problems. *Computers & Structures*, 142:1–14, 2014.

[12] R Hiptmair, A Moiola, and I Perugia. A survey of Trefftz methods for the Helmholtz equation. *arXiv preprint arXiv:1506.04521*, 2015.

[13] M E Honnor, J Trevelyan, P Bettess, M El-hachemi, O Hassan, K Morgan, and J J Shirron. An integration scheme for electromagnetic scattering using plane wave edge elements. *Advances in Engineering Software*, 40(1):58–65, 2009.

[14] T Huttunen, P Monk, F Collino, and J P Kaipio. The ultra weak variational formulation for elastic wave problems. *Society for Industrial and Applied Mathematics Journal on Scientific Computing*, 25:1717–1742, 2004.

[15] J M Jin. *The finite element method in electromagnetics.* Hoboken, N.J.: Wiley, 2014.

[16] I Kalashnikova, R Tezaur, and C Farhat. A discontinuous enrichment method for variable-coefficient advection–diffusion at high péclet number. *International Journal for Numerical Methods in Engineering*, 87(1-5):309–335, 2011.

[17] H Kohno, K J Bathe, and J C Wright. A finite element procedure for multiscale wave equations with application to plasma waves. *Computers and Structures*, 88(1):87, 2010.

[18] O Laghrouche, P Bettess, and R J Astley. Modelling of short wave diffraction problems using approximating systems of plane waves. *International Journal for Numerical Methods in Engineering*, 54(10):1501–1533, 2002.

[19] O Laghrouche, P Bettess, E Perrey-Debain, and J Trevelyan. Wave interpolation finite elements for Helmholtz problems with jumps in the wave speed. *Computer methods in applied mechanics and engineering*, 194(2):367–381, 2005.

[20] T Luostari, T Huttunen, and P Monk. The ultra weak variational formulation using bessel basis functions. *Communications in Computational Physics*, 11(02):400–414, 2012.

[21] J M Melenk and I Babuška. The partition of unity finite element method: Basic theory and applications. *Computer Methods in Applied Mechanics and Engineering*, 139(14):289 – 314, 1996.

[22] M S Mohamed, O Laghrouche, and A El-Kacimi. Some numerical aspects of the PUFEM for efficient solution of 2D Helmholtz problems. *Computers and Structures*, 88:1484–1491, 2010.

[23] M S Mohamed, M Seaid, J Trevelyan, and O Laghrouche. Time-independent hybrid enrichment for finite element solution of transient conductionradiation in diffusive grey media. *Journal of Computational Physics*, 251(0):81 – 101, 2013.

[24] M S Mohamed, M Seaid, J Trevelyan, and O Laghrouche. An enriched finite element model with q-refinement for radiative boundary layers in glass cooling. *Journal of Computational Physics*, 258(0):718 – 737, 2014.

[25] E Perrey-Debain, J Trevelyan, and P Bettess. Plane wave interpolation in direct collocation boundary element method for radiation and wave scattering: numerical aspects and applications. *Journal of Sound and Vibration*, 261:839–858, 2003.

[26] E Perrey-Debain, J Trevelyan, and P Bettess. Use of wave boundary elements for acoustic computations. *Journal of Computational Acoustics*, 11:305–321, 2003.

[27] E Perrey-Debain, J Trevelyan, and P Bettess. Wave boundary elements: a theoretical overview presenting applications in scattering of short waves. *Engineering Analysis with Boundary Elements*, 28:131–141, 2004.

[28] D M Pozar. *Microwave Engineering*. Wiley, 2004.

[29] M S Mohamed, M Seaid, J Trevelyan, and O Laghrouche. A partition of unity fem for time-dependent diffusion problems using multiple enrichment functions. *International Journal for Numerical Methods in Engineering*, 93(3):245–265, 2013.

[30] T Strouboulis, I Babuška, and R Hidajat. The generalized finite element method for Helmholtz equation: Theory, computation, and open problems. *Computer Methods in Applied Mechanics and Engineering*, 195:4711–4731, 2006.

[31] T Strouboulis, R Hidajat, and I Babuška. The generalized finite element method for Helmholtz equation part II: Effect of choice of handbook functions, error due to absorbing boundary conditions and its assessment. *Computer Methods in Applied Mechanics and Engineering*, 197:364–380, 2008.

[32] A Taflove. *Computational Electrodynamics: The Finite-difference Time-domain Method*. Antennas and Propagation Library. Artech House, 1995.

[33] A Taflove and M E Brodwin. Numerical solution of steady-state electromagnetic scattering problems using the time-dependent Maxwell's equations. *IEEE Transactions on Microwave Theory and Techniques*, 23(8):623–630, Aug 1975.

[34] R Tezaur, I Kalashnikova, and C Farhat. The discontinuous enrichment method for medium-frequency Helmholtz problems with a spatially variable wavenumber. *Computer Methods in Applied Mechanics and Engineering*, 268:126–140, 2014.

[35] H Wu and Z L Li. Scale issues in remote sensing: A review on analysis, processing and modeling. *Sensors*, 9(3):1768, 2009.

[36] K Yee. Numerical solution of initial boundary value problems involving Maxwell's equations in isotropic media. *IEEE Transactions on Antennas and Propagation*, 14(3):302–307, May 1966.